Electronic supplementary materials *Mendeleev Commun*., 2015, **25**, 468−469

Characterization of the electrocatalytic activity of carbon-supported platinum-based catalysts by thermal gravimetric analysis

Igor N. Leontyev, Daria V. Leontyeva, Alexandra B. Kuriganova, Yurii V. Popov, Olga A. Maslova, Nadezhda V. Glebova, Andrei A. Nechitailov, Natalia K. Zelenina, Alexander A. Tomasov, Louis Hennet and Nina V. Smirnova

Experimental

The preparation of Pt/C, Pt_3Co/C and Pt_3Ni/C catalysts was carried out using the electrochemical dispersion technique. The electrochemical cell has two metal (Pt, Pt_3Co or Pt_3Ni) foil electrodes 0.25 mm thick immersed into a suspension 2 M NaOH aqueous solution with the carbon black Vulcan XC-72 (Cabot Corp., USA) which was used as support. The electrodes were connected to pulse alternating current source operating at 50 Hz. Pt loading in the catalyst was controlled by the current amplitude and duration of the synthesis process. Finally, the freshly prepared catalyst was rinsed with H_2O to a neutral pH and dried at 80°C for 1 h.

The X-ray diffraction (XRD) studies were performed on the Swiss-Norwegian beam lines at the European Synchrotron Radiation Facility (SNBL ESRF) using a monochromated radiation (λ =0.72287 Å) and the Mar-345 Image Plate detector. The wavelength, sample-to-detector distance and resolution of the setup were calibrated with LaB6 powder (NIST). The samples were loaded into glass capillaries (Hilgenberg GmbH) with a diameter of 0.3 mm and a wall thickness of 0.01 mm.

The Raman measurements have been performed at a room temperature using a micro-Raman system inVia Reflex Renishaw in a backscattering configuration. The spectra have been excited with an Ar laser at a wavelength of 488 nm and collected under a microscope with a 100× objective. The Raman-scattered light was dispersed by a holographic grating with 2400 lines/mm and detected by a charge-coupled device camera. The instrument control was performed with the software package Renishaw WiRE. The Raman curve fitting for the determination of the spectral parameters was done using the Voigt function.

TEM investigations of synthesized catalysts were performed using the Carl Zeiss LEO 912 AB microscope. Energy dispersive X-ray microanalysis (EDAX) was carried out on a EDX

Zeiss LEO SUPRS 25. The thermogravimetric analysis was performed on a Mettler-Toledo TGA/DSC 1 thermal analyzer using STAR System software for data processing. The sample (around 50 mg) was heated from 308 to 1273 K at a heating rate of 5, 10 and 15 K min^{-1} under purified air flow rate of 30 cm^3 min^{-1}.

The fuel cell tests of the prepared Pt_3Ni/C, Pt_3Co/C and Pt/C with different Pt loading materials were carried out in a single PEMFC with a 1 cm^2 geometric area of the electrodes using the P-150 potentiostat (Elins) in an oxygen/hydrogen system (wetting 100%, temperature 296-297 K). The membrane electrode assembles, in which cathode contained Pt_3Ni/C, Pt_3Co/C and Pt/C with different Pt loading (20, 35, 46%) synthesized catalyst with a metal loading of 0.4 mg_{Pt} cm^{-2}, were manufactured on the membrane Nafion®212 by an airbrushing method [1].

Structural characterization

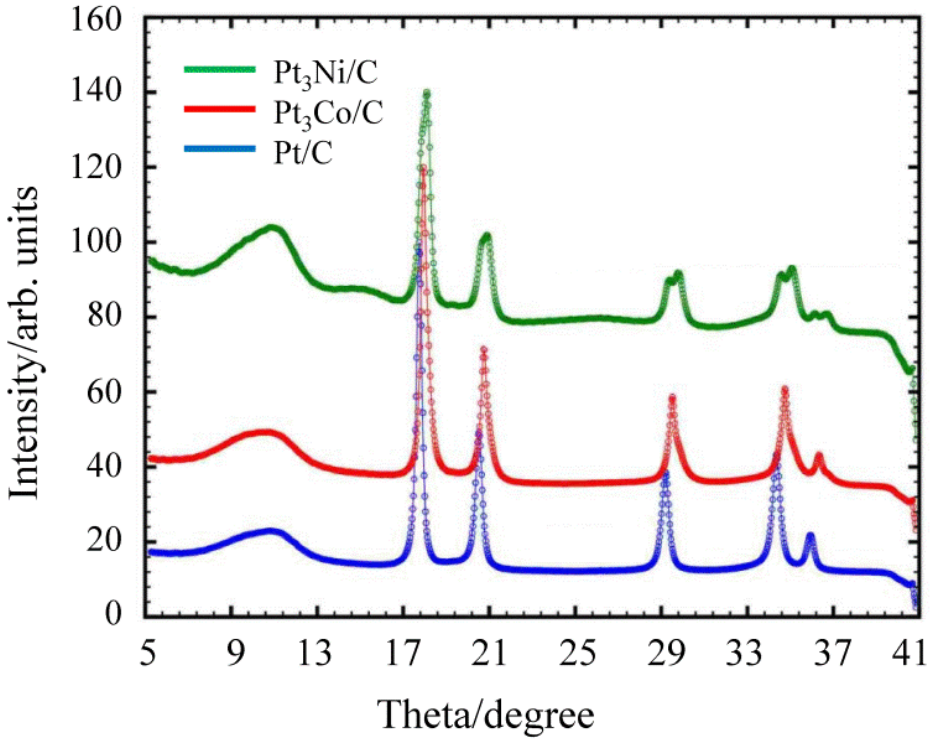

Figure S1 XRD powder patterns of the as-prepared Pt/C, Pt_3Ni/C and Pt_3Co/C catalysts.

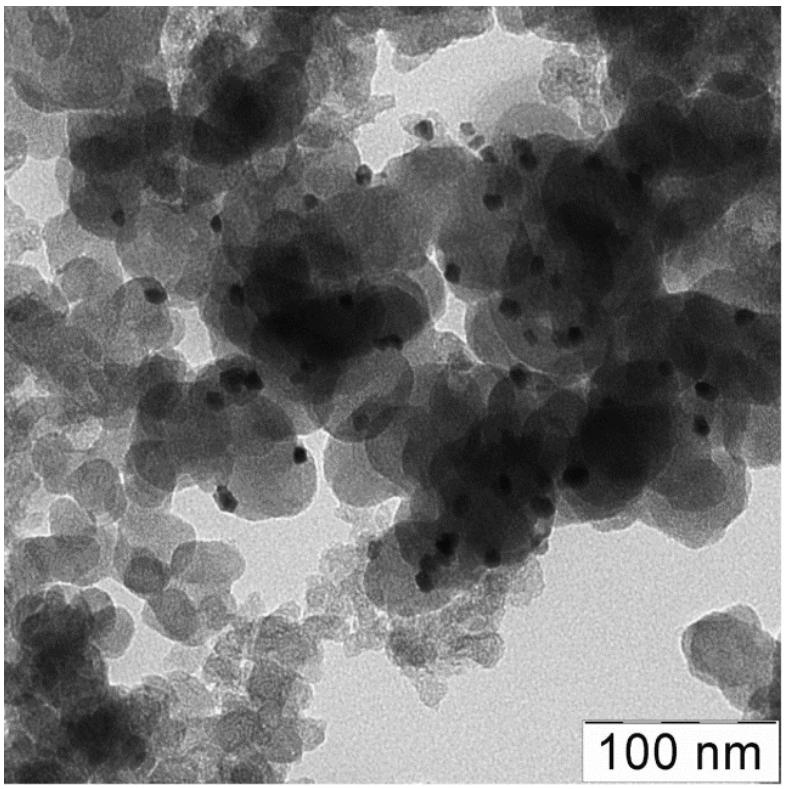

Figure S2 TEM images of Pt/C catalyst.

Table S1 Properties of as-prepared catalysts.

Sample	Metal loading, %			Max power density of MEA, $P_{max,}$ mW cm^{-2}	Onset temperature of carbon oxidation T_{onset}, K	Correlation coefficient R for plots of $\ln(\beta/T^2_m)$ against $1000/T_m$ (Figure S5)
	Theory	EDAX	TGA			
Vulcan XC-72	-	-	-	-	764	0,982
Pt_3Ni/C	27.0	22.5	23.7	94	700	0,974
Pt_3Co/C	28.8	27.2	28.0	112	634	0,996
Pt(20)/C	22.0	21.1	19.9	117	575	0,996
Pt(35)/C	35.0	34.8	35.4	250	518	0,996
Pt(46)/C	46.0	45.9	46.0	317	502	0,987

Kinetic analysis

All kinetic methods assume that for heterogeneous solid-state reactions, the rate of degradation or conversion dα/dt is a linear function of a temperature-dependent constant *k(T)*,

and the temperature-independent function of conversion *f(α)* (reaction model). It can be expressed as follows:

$$\frac{d\alpha}{dt} = k(T)f(\alpha) \qquad (1)$$

where *t* is the time, *T* is the absolute temperature, and *α* is the conversion fraction. The temperature dependence of the reaction rate is typically parameterized through the Arrhenius equation [2]:

$$k(T) = Ae^{-E_a/RT} \qquad (2)$$

where E_a is the activation energy of the oxidation process, A - pre-exponential (frequency) factor, R is the gas constant. Furthermore, for experiments in which samples are heated at a constant rate, the explicit time dependence of Eq.2 can be eliminated through the trivial transformation:

$$\frac{d\alpha}{dT} = \frac{A}{\beta} f(\alpha)\, e^{-E_a/RT} \qquad (3)$$

where β= dT/dt is the heating rate. For non-isothermal conditions, several relationships can be used to compute Arrhenius parameters (A and E_a), each of which is based on an approximate form of the temperature integral that results from rearrangement and integration of Eq.3. One such approximation gives rise to the Kissinger equation [3]:

$$\ln\left(\frac{\beta}{T_m^2}\right) = \ln\left(\frac{AR}{E_a}\right) - \frac{E_a}{RT_m} \qquad (4)$$

which is based on a model-free non-isothermal method where one does not need to calculate E_a for each conversion value in order to evaluate kinetic parameters. It allows to obtain the value of apparent activation energy E_a from the slope plot of $\ln(\beta/T^2_m)$ against $1000/T_m$ for a series of experiments at different heating rates β (Figure S3), where T_m is the temperature peak of the DTG curve (shown in Figure S 4b). Measurements were carried out at relatively high sample heating rates up to 15 K min^{-1}. However, all dependences are linear and the correlation coefficients R are close to 1 (see Table S1), which makes the data reliable.

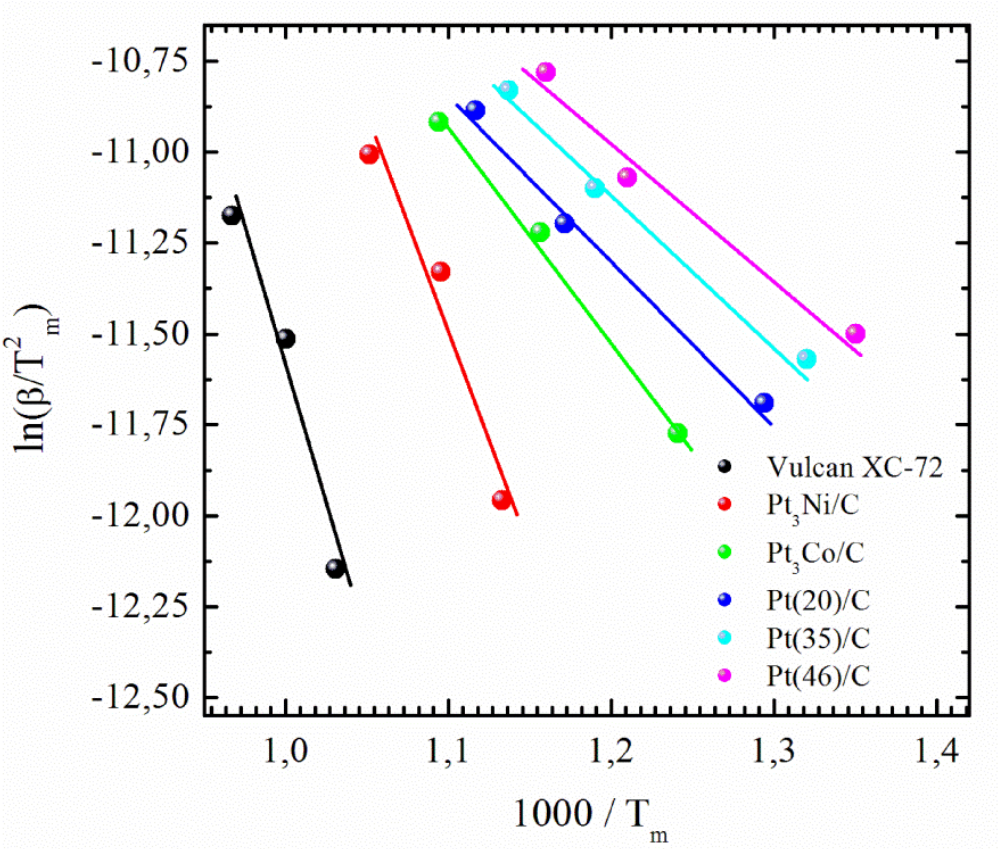

Figure S3 Kinetic curves of the pure carbon and metal-carbon catalysts oxidation.

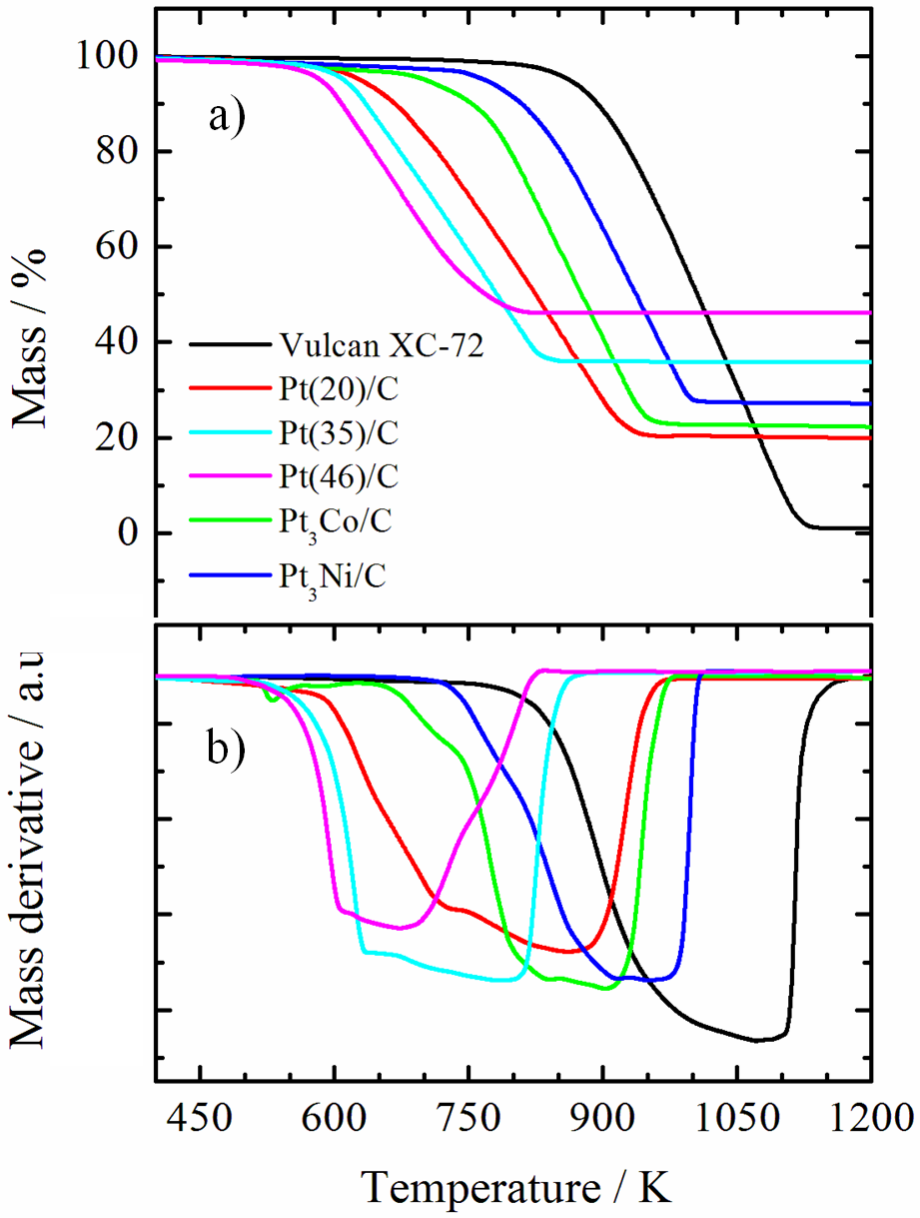

Figure S4 TG (a) and DTG (b) curves of Vulcan XC-72 and synthesized metal-carbon catalysts (β = 10 K min^{-1}).

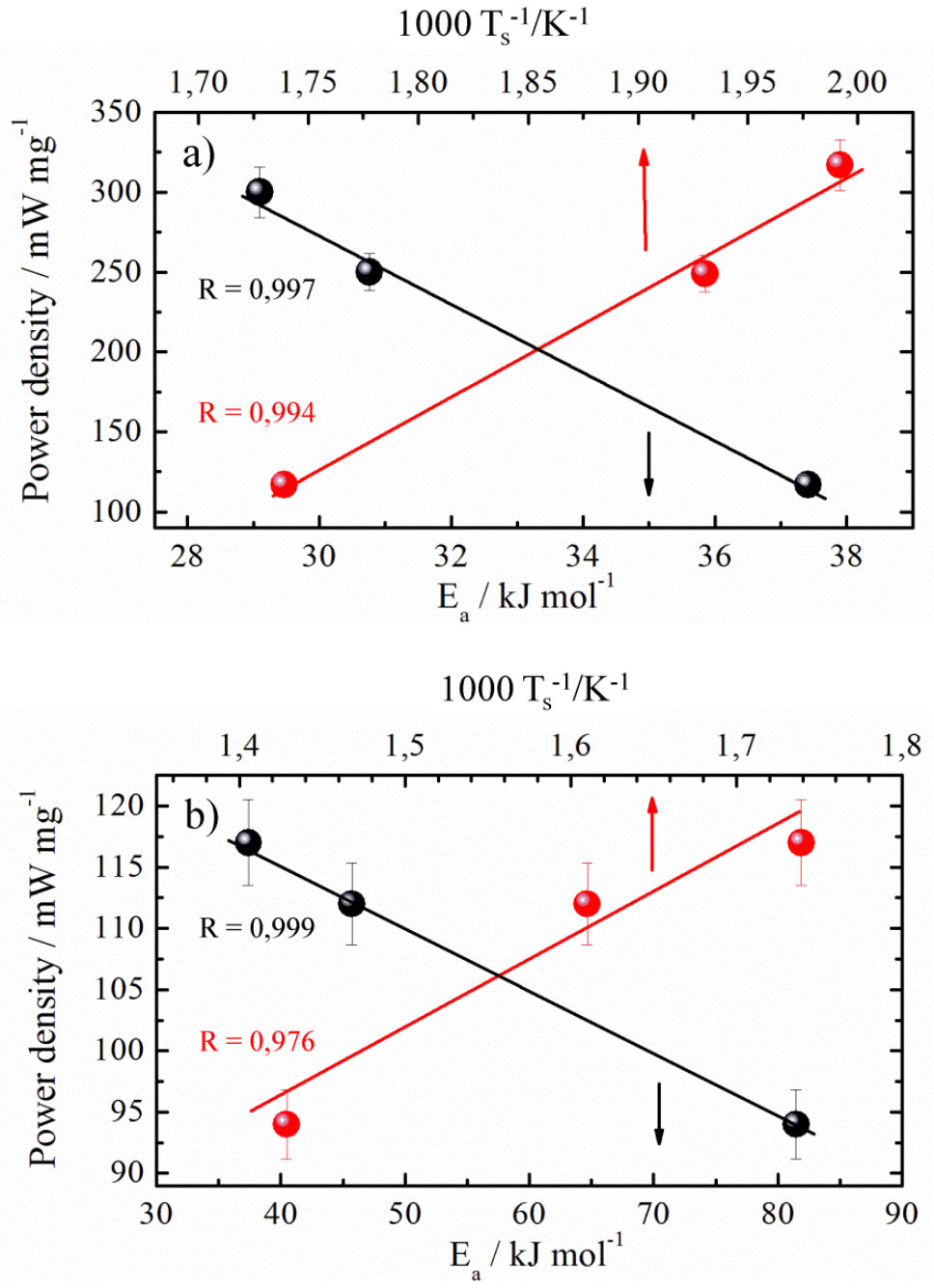

Figure S5 MEA power density vs. apparent activation energy E_a (black line) and the inverse onset temperature T_{onset} of carbon oxidation (red line) (a) of Pt/C with different Pt loading and (b) of Pt(20)/C and alloyed catalysts.

Certainly, using this approach only apparent activation energy of carbon oxidation can be calculated. This is evidenced by the complexity shape of the DTG curves in Figure S4b. Guterman [4] shows that the shape of DTG curves is determined not only by loading of platinum in the catalyst but also metal particles size distribution, their agglomeration, etc. These and many other parameters influence to the mechanism and kinetics of the catalytic oxidation of carbon, and in different temperature ranges character of this influence can vary considerably. In

addition, the kinetics of the carbon oxidation, including onset temperature of carbon oxidation is determined not only by the presence of catalytically active metals on the surface, but also pre-treatment conditions during catalyst preparation. In our case, the synthesis was carried out in alkaline solution with high concentration. Under these conditions, on the surface of carbon are formed a lot of oxygen-containing functional groups [4], which are influence to carbon combustion. In this paper, we calculate the apparent activation energy, which is only meaningful for comparative oxidation analysis of a series of catalysts prepared by one method on the same carbon support. Results are presented in Figure S5. The apparent activation energy E_a estimated to be 116 kJ mol^{-1} for the as-obtained Vulcan XC-72 is consistent with previously published data [5]. Presence of pure Pt and alloyed nanoparticles on the Vulcan XC-72 surface led to a remarkable decrease on the apparent activation energy. Thus, the catalytic activity of the prepared catalysts correlates not only with the onset temperature T_{onset} but also with the activation energy of carbon support thermal oxidation. Additionally, as it can be clearly seen (Figure S5), both dependences of power density on inverse onset temperature $1/T_{onset}$ and apparent activation energy E_a are well approximated with strait lines with coefficient correlation 0,997 and 0,999 respectively.

Raman spectroscopy

Raman spectroscopy is well known as a powerful tool for estimating the structural disorder in carbonaceous materials based on the intensities ratio of two spectral bands: the D band located at ~ 1350 cm^{-1} and induced by disorder in the carbon matter, and the so-called G band arising at ~ 1581 cm^{-1} due to the C-C stretching vibrations in the aromatic layers (the double-degenerate E_{2g} mode at the Brillouin zone center) and thus being Raman-active for sp^2 carbon networks. This ratio mostly denoted as I_D/I_G has been frequently used since 1970s [6, 7] to quantify the structural disorder of carbon. It is known that physical [8] and chemical treatment [9], as well as the catalyst particles precipitation, may strongly affect the crystal structure of carbon, leading to the increase or decrease of the defects concentration and hence cause the changes in its Raman spectrum. Thus, the effects of annealing at different temperatures and functionalization by Pt particles on structural ordering degree in carbonaceous material were shown in [10]. Furthermore, we have also performed Raman investigations of the Vulcan XC-72 sample preliminarily treated with NaOH and then dried at 80°C with the aim to highlight the treatment influence on the defectiveness of this material. It should be noted that the carbon support is subjected to a similar treatment during the Pt/C catalyst synthesis [1].

Figure S6 displays the Raman spectra of the bare, processed with NaOH and decorated by Pt nanoparticles Vulcan XC-72 samples. Here, several prominent Raman peaks typical of nanosized

carbon are clearly observed. The first-order spectral range (1000-2000 cm^{-1}) exhibits both D and G peak arising at 1357 and 1594 cm^{-1}, respectively. The rather high intensity of the G band compared to the D peak indicates a large quantity of defects on the surface, in particular, carbon nanoparticles and amorphous carbon clusters. One can also observe the appearance of an additional broad lines in the spectral range 2000-3500 cm^{-1} attributed to the second-order Raman scattering. The first one located at ~ 2700 cm^{-1} and denoted as 2D (or sometimes called G´) band corresponds to the overtone of the D band. The second one about 2950 cm^{-1} is associated with a D+G combination mode and is also activated by disorder [11].

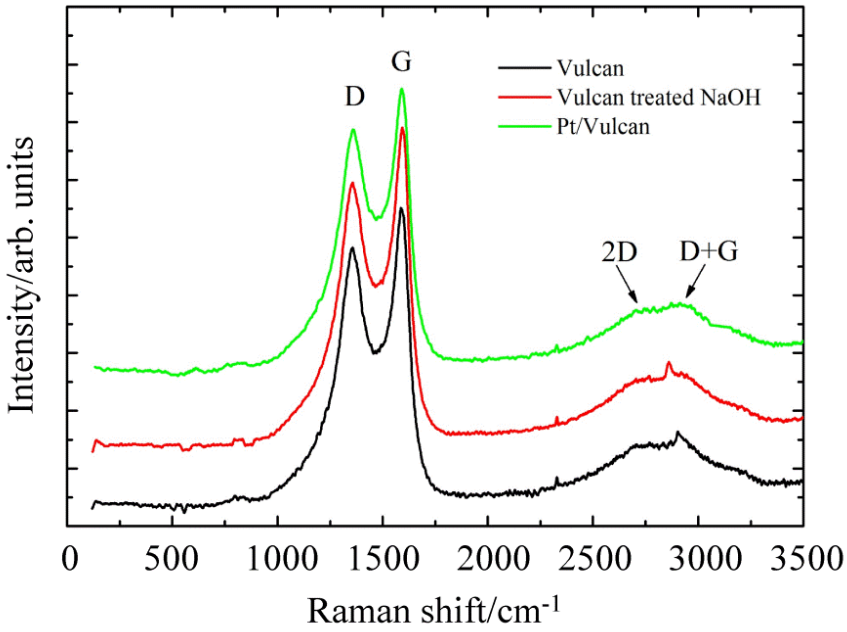

Figure S6 Raman spectra of the bare, NaOH-treated, and decorated by Pt nanoparticles Vulcan XC-72 samples.

To evaluate the crystallinity degree of the samples, the Raman spectra, preliminary corrected for background, have been fitted using a Voigt function with the aim to extract the integral intensities values of the bands D and G. For the as-obtained and treated with NaOH Vulcan XC-72, we determined a ratio I_D/I_G of 1.87 and 1.46, respectively. According to [10], this reduction observed for the treated Vulcan XC-72 is explained by increase of the structural order accompanied by a decrease of the defects amount at the surface of the sample after the thermal treatment. For the platinized Vulcan XC-72, the parameter I_D/I_G reaches the value of 1.97, indicating an increase of defect concentration at the surface of the graphite layer.

The defectiveness increase the carbon materials decorated with nanoparticles compared to the bare carbon was also observed in Refs [12, 13]. For example, in the oxidized MWCNTs [12] the activation energy E_a increases from 206 to 221 kJ mol^{-1}, while the parameter I_D/I_G shows a

five-fold increment. Furthermore, it was shown in [13] that for the CNTs synthesized at various temperatures the ratio I_D/I_G increases from 2.21 up to 3.60, while the onset oxidation temperature decreases by approximately 15-20 K. So, these results suggest that the drop of 262 K of the onset temperature of Pt(46)/C and the decrease of the activation energy of carbon oxidation observed in our case cannot be attributed to the increase of carbon defectiveness degree after coating with platinum nanoparticles.

A second theory assumed that the carbon support decorated by Pt nanoparticles was oxidized more rapidly than by O_2 coming from the gas phase due to effect named spill-over [14]. Such approach was used to explain the acceleration of coke removing from the oxide surface in presence of Pt nanoparticles [15] and the decrease of the temperature of maximum consumption rate for platinized boron-doped ultrananocrystalline diamond powder compared to the bare powder.

In absence of catalyst, the mechanism of the cooperative reaction proceeds via the adsorption of O_2 at the carbon surface to form intermediate -C(O) complexes [16] which do not decompose at a significant rate below 400°C (reaction 1).

$$C + O_2 \rightarrow 2\text{-}C_{sub}(O) \qquad \text{reaction 1}$$

The mechanism of carbon oxidation in the presence of Pt nanoparticles may proceed, as follows. As shown in Figure S7, oxygen molecule is first adsorbed dissociatively at the surface of the noble metal nanoparticles (reaction 2).

$$Pt + 0.5O_2 \rightarrow Pt\text{-}O \qquad \text{reaction 2}$$

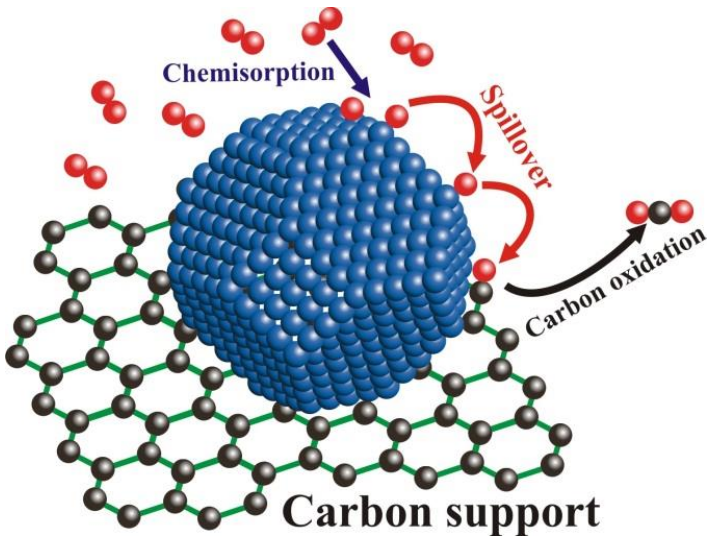

Figure S7 Schematic illustration of catalytic gasification of carbon support. Blue spheres are Pt atoms, red spheres are oxygen atoms and black spheres are carbon support.

At elevated temperature, the chemisorbed O atoms that formed on Pt are mobile and can migrate from metal to nearby carbon sites for its oxidation (reaction 3).

$$Pt\text{-}O + C_{sub} \rightarrow Pt + C_{sub}(O) \qquad \text{reaction 3}$$

The oxygen atoms then react with the carbon atoms to produce oxide functionalities, and the oxidation continues to produce CO_2 (reactions 4-6).

$$Pt\text{-}O + C_{sub}(O) \rightarrow Pt + C_{sub}(O)_2 \qquad \text{reaction 4}$$

$$C_{sub}(O)_2 \rightarrow CO_2 \qquad \text{reaction 5}$$

$$C_{sub}(O) + C_{sub}(O) \rightarrow C_{sub} + CO_2 \qquad \text{reaction 6}$$

In this case, the catalytic effect of the metal particle would partially depend on the thermodynamics of oxidation and would thus vary from one element to another, suggesting a possible reason for the differences between the observed catalytic effects of each metal on the carbon.

References

1. N.V. Smirnova, A.B. Kuriganova, D.V. Leont'eva, I.N. Leont'ev and A.S. Mikheikin, *Kinet. Catal*, 2013, **54**, 255 (Kinet. Katal., 2013, **54**, 265).
2. S. Vyazovkin and C.A. Wight, *Annu. Rev. Phys. Chem.*, 1997, **48**, 125.
3. H.E. Kissinger, *Anal. Chem.*, 1957, **29**, 1702.
4. V.E. Guterman, S.V. Belenov, V.V. Krikov, L.L. Vysochina, W. Yohannes, N.Yu. Tabachkova and E.N. Balakshina, *J. Phys. Chem. C*, 2014, **118**, 23835.
5. N.V. Glebova, A.A. Nechitailov, Yu.A. Kukushkina and V.V. Sokolov, *Tech. Phys. Lett.*, 2011, **37**(5), 438.
6. F. Tuinstra and J.L. Koenig, *J. Chem. Phys.*, 1970, **53**, 1126.
7. R. Saito, M. Hofmann, G. Dresselhaus, A. Jorio and M.S. Dresselhaus, *Adv. Phys.*, 2011, **60**, 413.
8. Zh. Shao, M. Pang, W. Xia, M. Muhler and Ch. Liang, *J. Energy Chem.*, 2013, **22**, 804.
9. W.M. Ashri, W. Daud and A.H. Houshmand, *J. Nat. Gas Chem.*, 2010, **19**, 267.
10. O.A. Maslova, A.S. Mikheykin, I.N. Leontiev, Yu.I. Yuzyuk and A.G. Tkachev, *J. Nanoelectron. Optoelectron.*, 2012, **7**, 95.

11. A. C. Ferrari and J. Robertson, *Phys. Rev. B.*, 2000, **61**, 14095.
12. M. A. Pimenta, G. Dresselhaus, M.S. Dresselhaus, L.G. Cancado, A. Jorio and R. Saito, *Phys. Chem. Chem. Phys*, 2007, **9**, 1276.
13. M. Lanza, S. Santangelo, G Messina, S. Galvagno and C. Milone, *ChemPhysChem*, 2010, **11**, 1925.
14. W.C. Conner Jr. and J.L. Falconer, *Chem. Rev*., 1995, **95**, 759.
15. M. Hara, M. Lee, C.-H. Liu, B.-H. Chen, Y. Yamashita, M. Uchida, H Uchida and M. Watanabe, *Electrochim. Acta*, 2012, **70**, 171.
16. E. Baumgarten and A. Schuck, *Appl. Catal.*, 1988, **37**, 247.